10-15-1997

Prototype for SONTRAC: a scintillating plastic fiber detector for solar neutron spectroscopy

James M. Ryan
University of New Hampshire, James.Ryan@unh.edu

Janis Baltgalvis
Science Applications International Corp.

D Holslin
Science Applications International Corporation

John R. Macri
University of New Hampshire - Main Campus, John.Macri@unh.edu

Mark L. McConnell
University of New Hampshire - Main Campus, mark.mcconnell@unh.edu

See next page for additional authors

Recommended Citation

James M. Ryan ; Janis Baltgalvis ; Daniel T. Holslin ; John R. Macri ; Mark L. McConnell ; Aaron R. Polichar and Cornelia B. Wunderer "Prototype for SONTRAC: a scintillating plastic fiber detector for solar neutron spectroscopy", Proc. SPIE 3114, EUV, X-Ray, and Gamma-Ray Instrumentation for Astronomy VIII, 514 (October 15, 1997); doi:10.1117/12.278901; http://dx.doi.org/10.1117/12.278901

A prototype for SONTRAC, a scintillating plastic fiber detector for solar neutron spectroscopy

James M. Ryan[a, 1], Janis Baltgalvis[b], Daniel Holslin[b], John R. Macri[a], Mark L. McConnell[a], Aaron Polichar[b], Cornelia B. Wunderer[a]

[a]Space Science Center, University of New Hampshire, Durham, NH 03824
[b]Science Applications International Corporation, San Diego, CA 92121

ABSTRACT

We report the scientific motivation for and performance measurements of a prototype detector system for SONTRAC, a solar neutron tracking experiment designed to study high-energy solar flare processes. The full SONTRAC instrument will measure the energy and direction of 20 to 200 MeV neutrons by imaging the ionization tracks of the recoil protons in a densely packed bundle of scintillating plastic fibers. The prototype detector consists of a 12.7 mm square bundle of 250 μm scintillating plastic fibers, 10 cm long. A photomultiplier detects scintillation light from one end of the fiber bundle and provides a detection trigger to an image intensifier/CCD camera system at the opposite end. The image of the scintillation light is recorded. By tracking the recoil protons from individual neutrons the kinematics of the scattering are determined, providing a high signal to noise measurement The predicted energy resolution is 10% at 20 MeV, improving with energy. This energy resolution translates into an uncertainty in the production time of the neutron at the Sun of 30 s for a 20 MeV neutron, also improving with energy. A SONTRAC instrument will also be capable of detecting and measuring high-energy gamma rays >20 MeV as a "solid-state spark chamber." The self-triggering and track imaging features of the prototype are demonstrated with cosmic ray muons and 14 MeV neutrons. Design considerations for a space flight instrument are presented.

Keywords: neutron, gamma-ray, solar, scintillating fibers, image intensifier, CCD

1. SOLAR PHYSICS MOTIVATION

Understanding the acceleration of particles to high energies is a key step in solving the solar flare problem. While it is clear that the energy source for particle acceleration is free energy in the non-potential magnetic fields in solar active regions,[1, 2]. many competing scenarios have been proposed for the mechanism(s) of particle acceleration,[3, 4]. A thorough understanding of the acceleration process requires a knowledge of the composition, energy distributions, angular distributions, spatial distributions, and production rates for energetic particles. These properties at the flare site are best determined by combined high spectral, temporal, and spatial resolution measurements of the radiation generated *at all energies* as the energetic particles interact with the solar atmosphere. While substantial observational and theoretical progress has been made during the last two solar cycles, gaining a complete understanding of the mechanism(s) of the particle acceleration process remains one of the key goals of solar physics research and it is unlikely to be achieved by a single instrument or mission. However, some nagging problems in solar particle acceleration can be addressed. These include (1) the rapid acceleration of high-energy electrons and protons (~1 s), (2) GeV proton acceleration (< 1 minute) and (3) the prolonged acceleration of GeV protons (~ 10 hours). To address these thornier problems, better measures of the proton spectrum are essential. This is the scientific question that can addressed with an orbiting solar neutron spectrometer. Whatever, the acceleration process is, it becomes inefficient at some maximum energy resulting in a break in the proton (or the electron) spectrum. With the SONTRAC instrument one can measure the break in the energetic proton spectrum by

[1] Corresponding author. Telephone: 603-862-3510; Fax: 603-862-4685; E-mail: James.Ryan@unh.edu

SPIE Vol. 3114 • 0277-786X/97/$10.00

comparing the flux of nuclear gamma rays to that of the neutrons from 20 to 250 MeV for many events beyond the few events known to have very high-energy emission. Measuring the most energetic parts of the neutron and photon (and thus the particle spectrum) provides the most secure handle on the fundamental processes of solar flare particle acceleration.

Unique information comes from detecting and measuring the distribution of particles at the highest energies. This is because the acceleration process is working at its greatest capacity, thus challenging theoretical models of the physics. The detection and measurement of high-energy solar emissions > 10 MeV gives us our best information about the process that accelerates ions and electrons out of the thermal pool of particles and up to relativistic energies. Solar neutrons are produced in solar flares by energetic protons (and other ions) accelerated in the corona that precipitate to the denser regions of the chromosphere or photosphere. These same energetic protons are responsible for nuclear gamma-ray emission and π meson production. The production of π mesons manifests itself in photon emission from the decay of neutral π mesons and through bremsstrahlung of the secondary electrons and positrons.

Both gammas and neutrons are neutral particles and their transport through the interplanetary medium is unaffected by the ambient magnetic field. Therefore, the production or release time of the gammas and neutrons can be calculated directly from the time-of-flight over one astronomical unit. In order to identify the origin time of the neutrons with respect to other solar flare emissions, the energy of the neutron must be known so as to propagate it backwards in time to the solar surface.

Nuclear gamma rays, neutrons and gamma rays associated with π mesons originate from different portions of the energetic proton spectrum at the Sun. Nuclear gammas from the electromagnetic decay of excited carbon, oxygen and other heavier nuclei primarily originate from the part of the proton spectrum just above the gamma-ray production threshold, typically around 20 MeV. A statistical correlation exists between the bremsstrahlung radiation from energetic electrons > 100 keV and nuclear-line gamma rays,[5] However, large scatter in the data suggest that significant differences exist between the efficiency of proton (or ion) and electron acceleration. Proton and ion spectra fall off with increasing energy, so that most of the protons are found at lower energies. The nuclear gamma-ray production is thus heavily weighted toward the low end of the spectrum due to the declining number of protons at higher energies and the fact that the gamma-ray production cross sections normally peak in the tens of MeV range. The threshold for production of π mesons from p-p collisions is around 300 MeV but is closer to 200 MeV for protons incident on heavier nuclei such as carbon. This means that information about the proton spectrum above 250 MeV can be derived from the emission of gamma rays associated with π meson production.

The intervening region of the proton spectrum (20–250 MeV) can only be measured by the detection and measurement of neutrons. This is a major gap in our knowledge and is filled only for a few exceptional flares with current orbiting instruments. Neutrons are produced at all energies above 10 MeV and retain some fraction of the energy of the protons (50% on average for subrelativistic neutrons) that produced them. Therefore, the measurement of neutrons in the range of 20 to 250 MeV can be related to the protons in that energy range.

The 2.223 MeV gamma ray line is a by-product of thermal neutron capture in the photosphere and serves as a rough monitor of the energy-integrated neutron flux. For example, an intense 2.223 MeV flux relative to the flux in the CNO nuclear line region (4–7 MeV) indicates a hard parent proton spectrum—the neutron production cross sections level out at high energies while the gamma-ray line cross sections are falling rapidly,[6] Although the 2.223 MeV line derives from thermal neutrons, it is a measure of the integrated broad-band neutron emission and is normally indicative of harder spectra.

Many flares (~100) exhibited nuclear gamma-ray emission as measured by the Gamma Ray Spectrometer (GRS) on the Solar Maximum Mission. However, few of them exhibited features associated with π meson or neutron production,[7] This is due to the fact that the neutron detection threshold for the GRS was around 100 MeV. The sensitivity rapidly declined below that energy. The small number of high-energy flares is also due, in part, to the wide variation in energetic proton spectra that flares possess. Inferred proton spectra from gamma-ray lines are generally well fit with exponential-like spectra,[8], but when high-energy emission is present at detectable levels, power laws are often required in the proton spectra in order to fit the data.[9] Flares

with hard and intense proton spectra will be the ones with gamma ray and neutron emissions above 100 MeV. All particle spectra eventually roll off at high energies. The roll off energy is determined by physical constraints, e.g., acceleration time, finite size of the acceleration region and loss mechanisms. Determining this roll-off energy for a number of flares, many of which may not exhibit π-related gamma-ray emission, will help estimate these physical parameters.

The COMPTEL instrument on the Compton Gamma Ray Observatory has begun to address this problem. It has measured the neutron flux from three flares in June 1991. Two flares analyzed in some detail are those of 9 and 15 June.[10, 11] The neutron emission on 9 June 1991 was 30× smaller than that of the well known flare of 3 June 1982.[7] However, the ability of COMPTEL to measure the energy of individual neutrons and thereby map them back in time to their production at the Sun reveals that most of the neutrons > 20 MeV were produced *after* the impulsive phase (and nuclear gamma rays) had significantly subsided. (Figure 1.) This indicates a hardening of the parent proton spectrum with time.[11] This level of neutron emission would have been undetectable with the GRS, especially given the high instrumental energy threshold. Even the large OSSE instrument with pulse-shape discrimination capabilities was unable to detect this flux.[12] In addition high-energy gamma rays consistent with a hard spectrum were detected with the EGRET instrument.[13] The ability of COMPTEL to perform this measurement and for us to conclude that high-energy acceleration is delayed stems from our ability to compute the kinematics of the neutron scatter within the instrument.[14, 15]

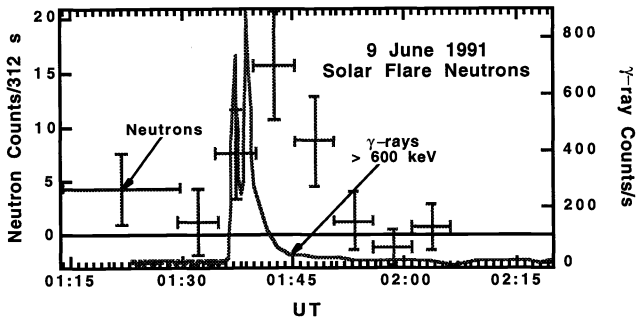

Figure 1: Neutron and γ-ray emission-time profiles for the 9 June 1991 solar flare, plotted at the time corresponding to a photon arrival time.

The solar flare of 15 June 1993 was not directly observed by any instrument. Both the GAMMA-1 high-energy gamma-ray telescope and the Compton Observatory were occulted by the earth during the impulsive phase of the flare. However, even though COMPTEL did not begin observing the Sun until 40 minutes after the peak X-ray flux, it was able to detect and measure neutrons from 15 to 80 MeV.[10] The lowest energy neutrons at the earliest observation times map back to the impulsive phase and are being used to estimate the intensity of the high-energy radiation from the impulsive phase.[10] Similarly, the other detected neutrons overlap in production time with the gamma rays measured by GAMMA-1 and are being used to limit the parent proton spectrum as it evolved. This illustrates the advantage of measuring the energy of individual neutrons over a period of time. Double-neutron elastic scattering in an organic scintillator is an established neutron spectroscopic technique, but it also allows one to determine the incident neutron direction if the direction of the first recoil proton is measured. COMPTEL only measures the recoil proton energy and the recoil neutron energy, but we can, on a statistical basis, still produce an image of a neutron source. Figure 2 is the image of the Sun after the 15 June 1991 solar flare produced from COMPTEL data. The geometrical constraints that are implicit in producing this image also provide a high S/N measurement of the spectrum. Measuring the direction of the first recoil proton would further increase the S/N ratio.

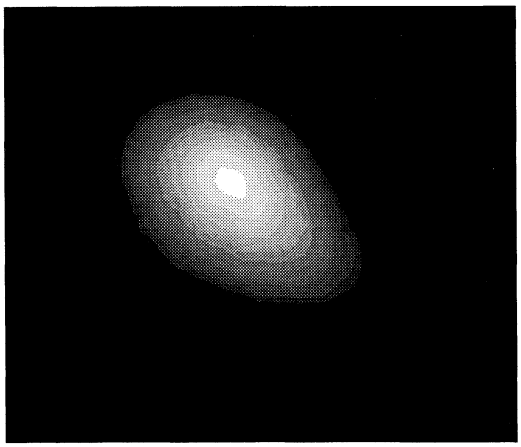

Figure 2. The image of the Sun in 10–80 MeV neutrons after the 15 June 1991 solar flare.

Unfortunately, COMPTEL is designed to measure gamma-rays and its neutron capability is secondary. (The earliest ancestors of COMPTEL were primarily neutron spectrometers and were later optimized for gamma detection.) An instrument designed specifically to measure the neutron flux would perform correspondingly better. A comprehensive attack on the high-energy proton acceleration problem relies on neutron measurements over a wide range of energies and gamma-ray measurements in the range of 2.223 MeV (^{2}H), 1–2 MeV (Ne, Mg, Si), 4–7 MeV (C, N, O) and > 20 MeV (primary and secondary electrons).

2. TRACKING DETECTOR CONCEPT

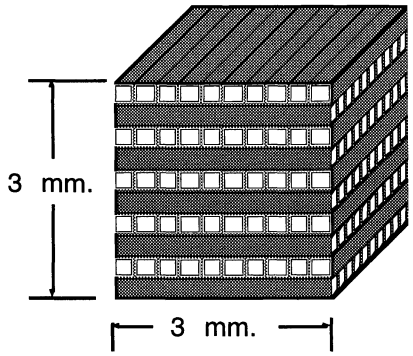

Figure 3. small segment of a proposed 22 cm cube fiber bundle, illustrating orthogonal scintillating fiber layers.

We have been investigating a new type of device for measuring solar neutrons in the 20 to 200 MeV range. The basic instrument concept consists of a closely packed bundle of square cross section organic plastic-scintillator fibers. Figure 3 represents a 3 mm cubic segment of such a bundle. The fibers are arranged in stacked planes with the fibers in each plane orthogonal to those in the planes above and below. This alternating orientation of fiber planes allows one to track ionizing particles in three dimensions from their origin to the point where they stop. The tracking detector measures the energy and direction of neutrons by imaging the ionization tracks of the recoil protons. The Bragg peak, stronger ionization near the end of the track, is used to determine track direction. Neutrons undergo elastic scattering off hydrogen within the organic plastic-scintillator fibers, scattering at right angles with respect to the scattered proton at non-relativistic energies. A second proton scatter of the scattered neutron provides spatial information that is necessary and sufficient to determine the incident neutron energy and direction. The scattered neutron with lower energy has a shorter mean free path, so it is likely to scatter a second time, providing the geometry information necessary to determine the kinematics. (The COMPTEL instrument, on the other hand, uses time-of-flight to determine the energy of the first recoil neutron. For SONTRAC the kinematics are entirely determined by geometry.) The non-relativistic double-scattering schematic in a solid block of plastic scintillator is shown in Figure 4. Once the kinematics are known an image of the neutron source can be constructed, e.g. Figure 2., and these data can then be used to create a neutron spectrum. The angular and energy resolution are dependent upon the ability to precisely track the recoil protons and measure the scintillation light.

The tracking detector's spectroscopic, track detection and imaging components are illustrated in Figure 5. These units cover the entire light emitting area of the bundle and are duplicated in the orthogonal dimension (not shown). The scintillation light signal is collected and processed at both ends of the fiber bundle. At one end a signal above threshold from the photomultipliers (PMT) fires a discriminator that in turn provides a signal to the trigger logic circuitry. At the other end of the fiber bundle fiber-optic tapers and a pair of image intensifiers demagnify, capture and hold the scintillation-light image of the ionization track(s) for readout by the CCD camera. The first image intensifier in this chain is always ON. Its phosphor holds the image for approximately 1 ms. The second image intensifier in this chain is normally in the gated-OFF condition and no image signal is passed to the CCD sensor. However, when the trigger logic registers the proper coincidence, the track image and PMT pulse height data are acquired and passed to an event builder and combined for subsequent event-by-event analysis.

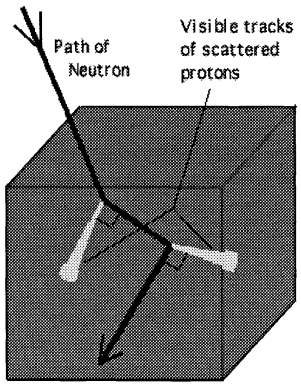

Figure 4. N-P kinematics. Schematic of non-relativistic double neutron scatter.

The fundamental instrument design was studied extensively with Monte Carlo simulations.[16, 17, 18] It suffered at the time from a lack of technology and existed in simulations only. This technology has been applied to high energy physics experiments,[19] and has since become available at a reasonable price. We have proposed a 22 cm cube tracking detector, derived from the earlier CWRU concept and the fundamental prototype engineering performed by UNH and Scientific Applications International Corporation (SAIC), for a NASA SMEX mission during the upcoming solar maximum. A description of the laboratory prototype follows.

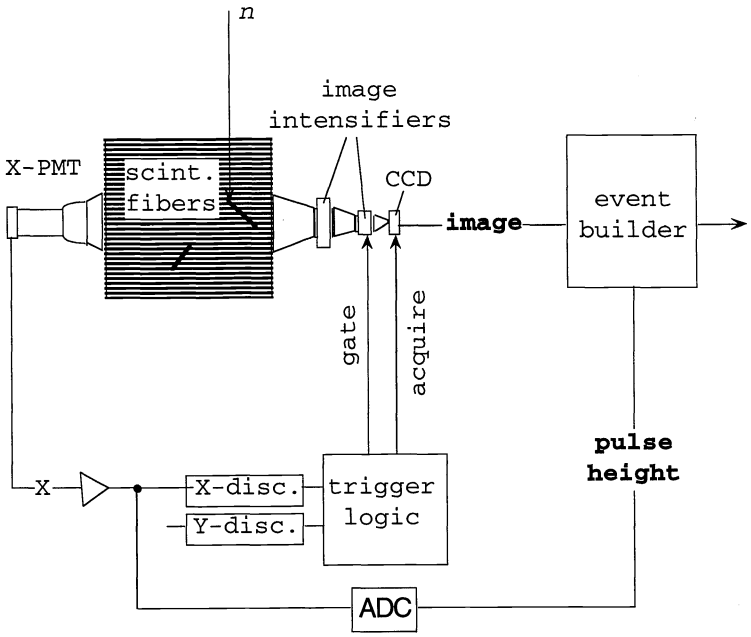

Figure 5. Major components of the tracking detector system. Orthogonal elements not shown.

3. PROTOTYPE DESCRIPTION AND TEST SETUP

The tracker prototype was developed to demonstrate the tracking capabilities and to begin to address fundamental science and engineering issues related to the calibration and design of space flight instrumentation.

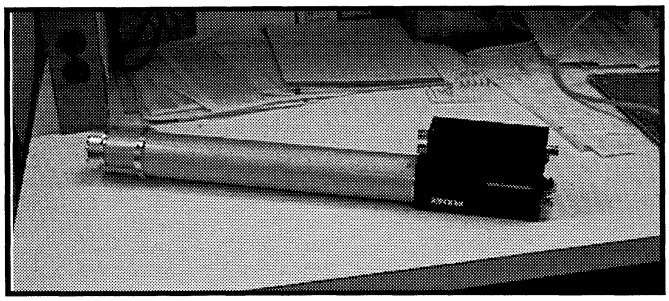

Figure 6. The SONTRAC prototype detector. The Pulnix camera (TM-9701) is shown to the right and the PMT to the left. SAIC built and tested the SONTRAC prototype detector for the Space Science Center at the University of New Hampshire.

Figure 6 is a photograph of the prototype tracker. Figure 7 is a schematic representation of its major components. It is assembled from commercially available parts which can be replaced or interchanged in performance tradeoff studies. To save cost it is small and limited to tracking in two dimensions. Larger scale, three-dimension tracking prototypes will follow when optimal parameters such as phosphor type(s) for the image intensifiers are determined.

Table 1 describes the configuration for the results reported here. It has a 10 cm long bundle of 250 μm square scintillating plastic fibers on 300 μm pitch within a 12.7 mm square envelope. The thickness of the scintillating fibers of the prototype was chosen such that a 10 MeV recoil proton traverses several fibers before stopping. The fiber pitch is 300 μm (including cladding and EMA) and the range of a 10 MeV proton (50% of the proposed neutron threshold energy) is 1.25 mm, equivalent to ~4 fibers. The PMT is a bialkali photocathode device from Thorn EMI. Two 18 mm diameter single MCP generation-2 image intensifiers from DEP are employed. The S20 photocathode for the first image intensifier was selected for optimum response to the scintillation light signal. The P43 phosphor will hold the image for approximately 3 ms (time to 1% brightness). The second intensifier's photocathode and phosphor were selected to provide a good spectral match to the output of the first intensifier and the input to the CCD sensor. The CCD camera (Pulnix TM-9701) is an inexpensive, progressive scanning camera with digital readout and control and asynchronous external trigger and full frame shutter capability. The frame grabber and image processor are from Matrox and operate in a Pentium PC. The logic and PMT signal amplifier circuitry consists of NIM-standard laboratory modules. The light from an internally mounted, externally

driven LED is seen by both the PMT and the imaging electronics and is available for setup and diagnostic testing. Measurements with the LED are used to help establish appropriate gains, gate delays and integration times and to determine the mapping of scintillating fiber boundaries onto the CCD.

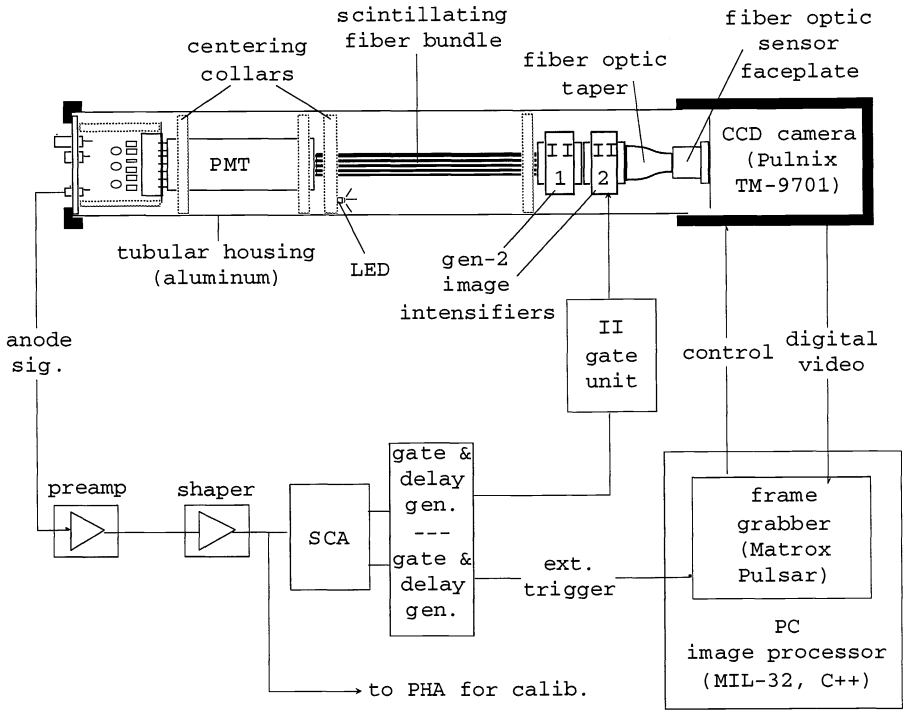

Figure 7. Schematic diagram of the SONTRAC prototype.

Table 1 **Tracking detector prototype (initial configuration)**		
scintillating fiber bundle	Bicron, BCF-99-55, multiclad, with black EMA	250 μm square fibers, 300 μm pitch 100 x 12.7 x 12.7 mm
image intensifier, 1st stage	DEP, XX1450LK, single MCP gen-2, 18 mm	S20 photocathode, P43 phosphor
image intensifier, 2nd stage	DEP, XX1450LJ, single MCP gen-2, 18 mm, gatable	S25 photocathode, P43 phosphor
CCD camera	Pulnix TM-9701	progressive scan, full frame asynchronous ext. trig. shutter, windowless imager
fiber optic taper and faceplates	Schott 32AS	taper ratio 18:6.4
photomultiplier (PMT)	Thorn EMI (9125B, 30 mm.)	bialkali, low noise glass
frame grabber	Matrox Pulsar	digital interface with camera
image processor	Matrox MIL-32	
trigger logic	various NIM modules	
intensifier gating unit	HiLight 2522	

4. PROTOTYPE PERFORMANCE

Our ability to track recoil protons has been demonstrated in the lab. A SONTRAC prototype was exposed to 14 MeV neutrons at San Diego State University. The tracks of recoil protons that will be near our trigger threshold energy are shown in Figures 8 and 9. On the left are the CCD camera image of the track and on the right are the same data that have been

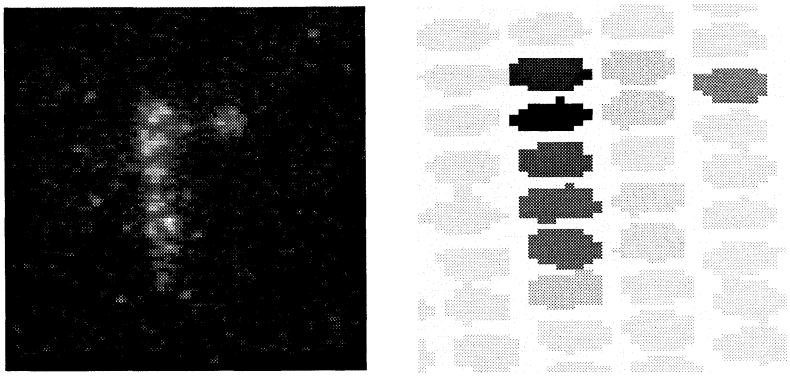

Figure 8. A ~11 MeV proton track image. Neutron incidence is from the bottom.

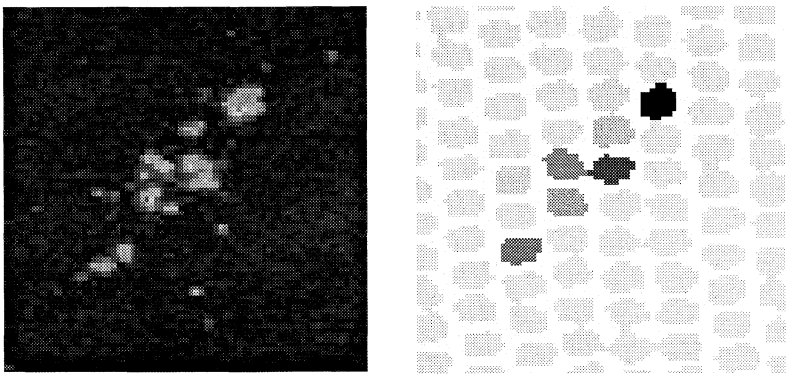

Figure 9. A ~11 MeV proton track image. Neutron incidence is from the bottom. The proton scattered at ~45°.

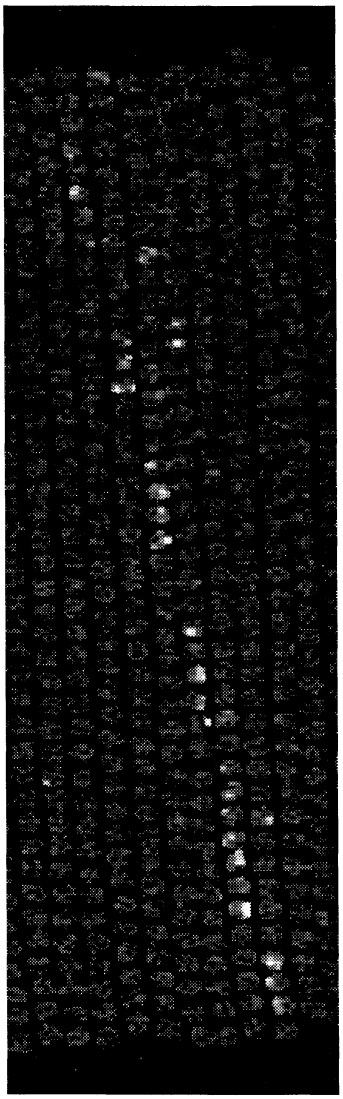

Figure 10. A cosmic-ray muon track. The vacant areas represent passive material.

binned into fibers containing the ionization. (The scintillating fiber boundaries are obtained by calibration.) The dynamic range of the fiber brightness expected from an 11 MeV proton is ~2. This agrees well with the density distribution in the figure. The direction of the proton is from the bottom of the figure to the top. The bright fiber to the right of the proton track in Figure 8 is probably a related second scatter. Near threshold energies and with tracking in only two dimensions with the prototype, more information is difficult to obtain.

Figure 10 is a minimum ionizing muon track measured with the SONTRAC prototype. The track image traverses the full 12.7 mm width of the fiber bundle. We calculate that the image intensifier should receive 19 scintillation photons from a minimum ionizing particle in a 250 μm fiber. This translates into ~4 photoelectrons/fiber for amplification within the image intensifier. (The intrinsic noise of the image intensifier is negligible.) Given that many co-linear fibers will have such a signal, we expect to be able to easily track minimum ionizing particles. The density of scintillation light from the minimum ionizing muon in Figure 6 is approximately what would be expected based on the density of the proton track in Figure 4 and is also consistent with the expected number of 4 photoelectrons/fiber. The sparse

nature of the muon track is due to passage through non-scintillating material (cladding and EMA) and Poisson statistics.

Figure 11 is the pulse height spectrum from the fiber bundle PMT recorded for muons incident normal to the fiber axis. Note that the muon peak is well defined and that its pulse height in our 12.7 mm thick fiber bundle represents approximately one fifth of the proposed trigger threshold.

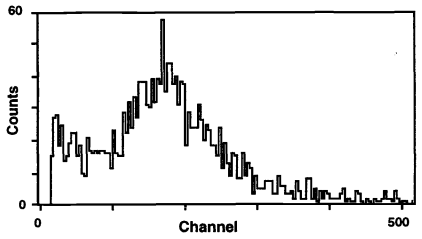

Figure 11. Muon spectrum from prototype tracker. Muons incident normal to fiber bundle axis. FWHM = 66%.

5. PROPOSED FLIGHT DESIGN

We have recently proposed a new NASA SMEX mission for studying high energy solar flare emission. The primary instrument will be a solar neutron tracking device. A conceptual sketch of the 22 × 22 × 22 cm tracker is shown in Figure 12.

Although we have only discussed the design and operation of the SONTRAC neutron telescope. Its use in space is greatly enhanced with data from supporting instruments. We envision that the neutron tracker would be accompanied by several high-efficiency gamma-ray spectrometers, perhaps using BGO for maximum efficiency, an X-ray spectrometer, and a gamma-ray polarimeter. Such a suite of instruments would fit within a NASA SMEX envelope. A schematic of such a payload is shown in Figure 8.

The detectors are located on the sun-facing side of the detector assembly which includes an active 4π charged particle anticoincidence shield surrounding the detectors and their supporting front end electronics (FEE).

The fiber block is surrounded by charged particle detectors to (1) reject cosmic ray protons and electrons and (2) to detect the escape of secondary charged particles from

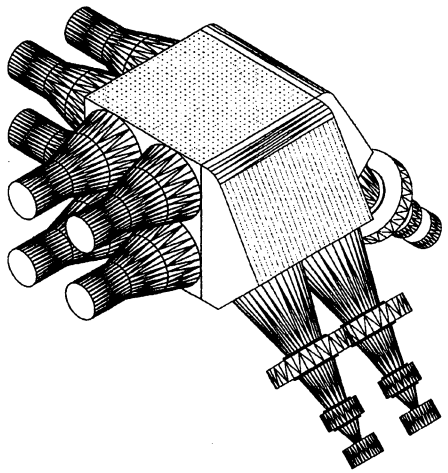

Figure 12. Conceptual sketch of a 22 × 22 × 22 cm scintillating plastic fiber tracking detector.

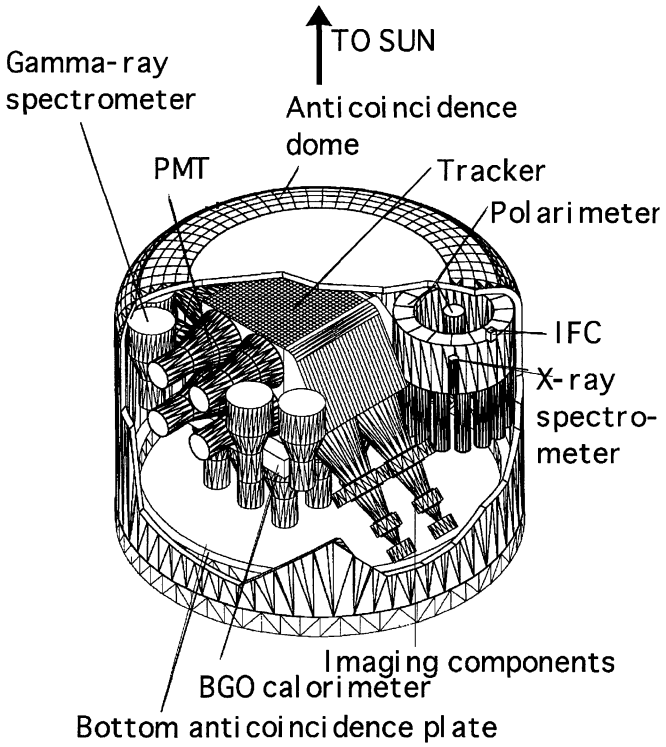

Figure 13. Cutaway isometric view of proposed SMEX payload and instruments.

reactions within the detector. Directly behind the fiber block is a BGO calorimeter, serving also as gamma-ray spectrometer. (The final choice of the detecting material may be NaI or CsI.) Although the detector can measure the energy and direction of neutrons < 250 MeV, fluxes of higher energy neutrons will be present in the most intense and energetic flares. These neutrons will most likely initiate complex inelastic n-C reactions producing a variety of neutral and charged secondaries. These secondaries will generally be forward beamed and can be detected with high efficiency by the BGO spectrometer. The very highest energy neutrons will produce secondaries that will pass through the calorimeter and out the charged particle anticoincidence shield behind the detector. Pulse height analysis will be performed on the BGO spectrometer and the back (bottom) plastic (anticoincidence) detector for events with coincident signals in the fiber block. The signals from the calorimeter and the back plastic detector provide an estimate of the number of escaping charged particles. This constitutes the high-energy neutron mode of the instrument, i.e., a signal in the fiber block detector with accompanying signals in the calorimeter and perhaps the back plastic charged particle shield. No signal must be present in the forward or side charged particle shields. The proposed instrument will be compact—basically a solid block of detecting material with a high ratio of active to passive material. The internal structure, alternating fiber planes, provides the detailed spatial information for tracking and analyzing fast proton paths. The "monolithic" structure provides a large solid angle for neutron-proton scattering, thereby increasing its efficiency. (The small solid angle factor of the n-p scattering in COMPTEL severely limits its efficiency.)

Extrapolating from Pendleton's calculations, [18], (Figure 14) we estimate (from volume arguments) that our $(22\ cm)^3$ cube concept would have an effective area of ~40 cm^2 from 15 to 60 MeV. This is more than 20× the effective area of COMPTEL for detecting and measuring neutrons. The typical energy resolution is on the order of 10% or better for the majority of neutron events. This results in an uncertainty in the production time of the neutron at the Sun of 30 s at 20 MeV. With increasing neutron energy a 10% energy uncertainty translates into smaller production time errors. (This is important in determining the production-time profile of neutrons that can then be compared to that of the gamma rays to identify spectral changes in the parent proton population.) The simulations also show that n-C interactions (elastic and inelastic) do not significantly interfere with the detection of neutrons via the n-p scattering process. The good spatial resolution of the detector provides one with the ability to distinguish between the two types of interactions, the n-C interactions showing a vertex with complex structure (several secondaries) as opposed to the isolated straight tracks produced by n-p events. Neutron-C scatters that produce no visible charged secondaries generally do not deflect the neutron trajectory enough to cause a serious error in the determination of the neutron energy via a subsequent n-p interaction.

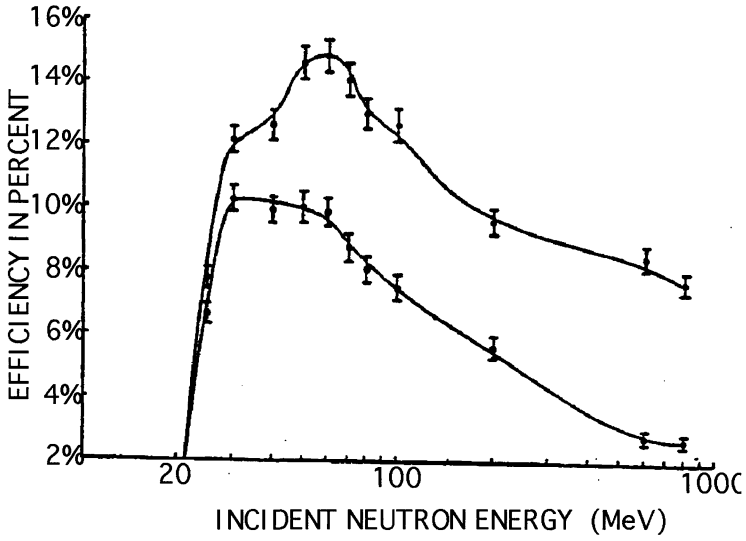

Figure 14. Calculated detector efficiency for a 50 cm cube as a function of incident neutron energy. Top curve: total efficiency for neutron energy reconstruction. Bottom curve: efficiency for neutron energy reconstruction with 10% of the correct energy. (Frye, et al., 1987)

Angular resolution is largely determined by the pitch of the fibers, i.e., the uncertainty in the end points of the particle tracks. For a 45° scatter it ranges from 23° at 20 MeV to ~5° at 50 MeV to 0.7° at 200 MeV. Although we will not be able to image the "hot" spots on the solar disk, this angular resolution is the basis for our high signal-to-noise ratio and thus our good sensitivity.

In front of the fiber block detector will be a thin (1 mm) Ta (or Pb) foil. It will serve to attenuate the X-ray flux below 200 keV, thereby reducing the pulse pile-up problem in the trailing detector elements. The high-Z foil also serves another function, i.e., to convert gamma rays > 20 MeV into electron-positron pairs. The electron pair can then be tracked within the fiber-scintillator block and if the electrons are energetic enough they will be absorbed by the calorimeter and measured. This technique of tracking converted electrons is employed successfully by spark chamber gamma-ray telescopes and cosmic-ray detectors.[20]

Although thin, the 1 mm Ta foil will produce a small number of neutron interactions (3% of incident neutrons), but these can be identified by proton tracks that begin at the Ta converter. The high-energy gamma-ray detection proceeds in the same manner as the high-energy neutron mode, i.e., the calorimeter and the back plastic charged-particle shield are utilized as detecting elements with no signals from the other charged particle shields.

Although we do not claim that this instrument will have the performance of a spark chamber telescope for detecting and measuring high-energy gamma rays, we note that the SONTRAC technology allows this telescope to count, track and record gamma rays at rates at ~100 Hz as opposed to a few per second for a spark chamber. This is important in measuring the gamma-ray flux during intense flares. The EGRET instrument, even if operating at the time, cannot measure gamma rays in its spark chamber during the impulsive phase of flares and its time resolution in its calorimeter is 32 s. Our high-energy gamma-ray telescope function of SONTRAC will far exceed the EGRET performance figures.

Monte Carlo simulations show that the efficiency of producing positron-electron pairs in the Ta converter or the plastic scintillator itself is approximately 40% from ~50 MeV up to 1 GeV. (Figure 15). Almost all the other gamma rays convert in the calorimeter, providing spectroscopic data for high-rate conditions.

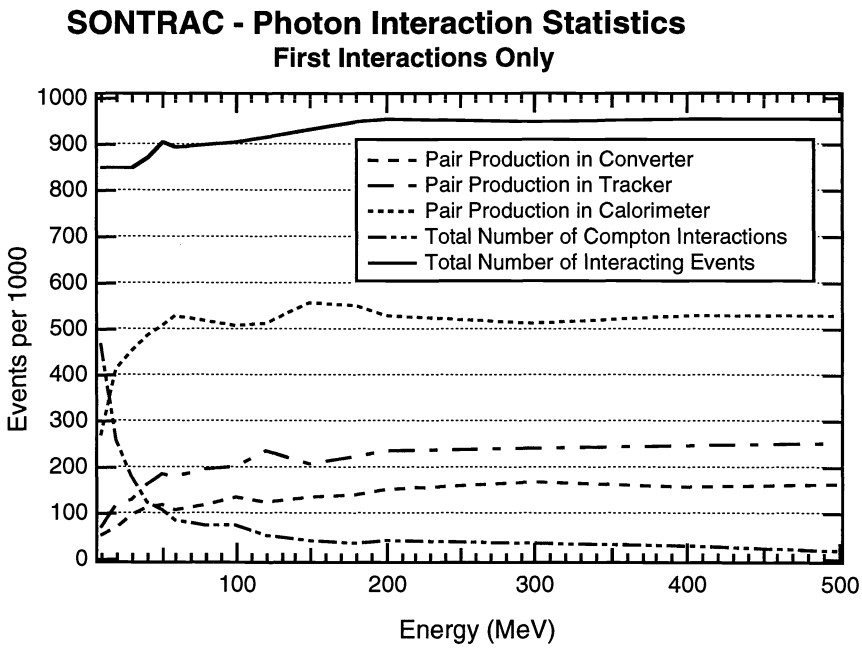

Figure 15. Results of efficiency simulations for gamma-ray detection in the proposed 22 cm cube tracking detector.

For the neutron flare of 3 June 1982, with an integrated flux of 7×10^{31} $E^{-2.4}$ MeV^{-1}-sr^{-1},[7] a $(22\ cm)^3$ detector would detect 2×10^4 neutrons over a period of 1200 s. This represents a rate of ~20 Hz, well below the on-board image processing limit of ~100 Hz. Although the triggering scheme is different, we expect that the signal-to-noise of the detector will be on the same order as that of COMPTEL since the technique (double scatter) is similar. Scaling COMPTEL neutron rates >20 MeV,[21] by the relative volumes, we estimate that SONTRAC will experience a background count rate of 5 s^{-1}, for a rate in the solar direction of 0.15 s^{-1}, but with 20× the effective area of COMPTEL. If we pessimistically assume that these are distributed isotropically and that our angular resolution is no better than 20°, then our

sensitivity is still 10× better than COMPTEL. The 9 June 1991 flare neutron signal would, in that case, approach 50 σ. We would consequently have a dynamic range in count rate of ~200. We could then readily measure neutron fluxes from numerous M class X-ray flares. To date only X class flares have exhibited detectable neutron emission.

The background that the tracker must endure in quiescent periods will be primarily from cosmic ray protons. Although cosmic ray protons will be identified by a trigger of the charged-particle veto system, the image of the track of such a proton will linger and may be present in the image of a legitimate neutron or gamma event. However, minimum ionizing tracks are clearly distinguishable from heavily ionizing neutron-recoil protons in our energy range. In short, good tracks will be identifiable in the context of cosmic-ray proton tracks. Even in the worst case, scaling from COMPTEL veto dome data, we only expect to encounter ~30 Hz of cosmic-ray tracks in the detector. This is one basis for our choice of an equatorial or low-inclination orbit—the contribution of cosmic-ray tracks is minimized.

The discrimination between neutron and gamma-ray events in the block should be close to 100%, because the gamma-ray induced reactions, Compton scattering and pair production, result in tracks that are minimum ionizing and show appreciable multiple scattering at low energy. Bias levels or thresholds can be set to identify most of these events. The high-energy gamma-ray mode will deal with electrons > 10 MeV where multiple scattering is greatly reduced. There the minimum ionizing nature of the tracks will identify gamma-ray events.

6. FUTURE WORK

We will continue to study the performance of the existing prototype tracker as part of our ongoing NASA SR&T work. More specifically, we plan to perform the following studies.

- Measure the muon track image signal-to-noise as a function of intensifier gains, gating delays and image integration time. This will help us to understand the tradeoffs and optimize performance.
- Incorporate a fiber optic taper before the first image intensifier to demagnify the image and assess the impact of the reduction in signal on achievable threshold and minimum ionizing track image signal-to-noise. Such studies will help to achieve large volume trackers with smaller less costly image intensifiers.
- Replace the present image intensifiers with similar models having different photocathodes and/or phosphors and compare performance. In particular, faster phosphors on the first intensifier will permit track detection at higher rates.
- Modify the PC data and image acquisition system to integrate the PMT pulse height measurement into each image event message. This will give us a better handle on important calibration issues.
- Perform calibration measurements at higher neutron energies.
- Develop models of detector response and compare predictions with prototype measurements.

We will also pursue development of a larger prototype tracker, 10 × 10 × 20 cm, with orthogonal layers of scintillating fibers and orthogonal electro-optics. This larger prototype will be more representative of a flight instrument and permit us to do the following.

- Address the engineering issues associated with construction, assembly and operation of a large orthogonal-layer tracker. These issues include mechanical tolerances, environmental constraints, and the relative performance of correspondingly larger opto-electronic elements.
- Develop algorithms for track identification and reconstruction in three dimensions
- Perform calibrations at higher energies with neutrons an gammas.
- Continue to develop and validate detector response models.

7. CONCLUSIONS

The SONTRAC laboratory prototype developed by UNH and SAIC under a NASA SR&T grant has demonstrated the important features of the detection technique not addressed in earlier work. This helped to determine the engineering parameters important to the SONTRAC application (scintillating fiber pitch, light yields, gains, photocathode and phosphor selection, gating delays and intervals). It is limited to tracking in

two dimensions. Self-triggered images of the tracks of recoil protons from 14 MeV neutrons and the minimum ionizing tracks of cosmic ray muons are clearly resolved. An extension to 3-dimensional tracking promises to provide unprecedented capabilities for studying the acceleration of energetic particles in solar flares.

8. ACKNOWLEDGMENTS

We wish to thank Professor Patrick Papin and his crew at San Diego State University for their assistance with the 14 MeV neutron calibration.

This work is supported under NASA's Space Physics Supporting Research and Technology program.

9. REFERENCES

1. Hagyard, M.J., et al., Advances in Space Research 4 (7 1984): 71.
2. Zirin, H. Astrophysics of the Sun. New York: Cambridge Univ. Press, 1988
3. Hudson, H. and J. Ryan. Annual Review Astronomy and Astrophysics 33 (1995): 239-82.
4. Vestrand, W.T. and J.A. Miller. Particle Acceleration During Solar Flares. Vol. in press. The Many Faces of the Sun: The Scientific Results of the Solar Maximum Mission, ed. B. Haisch et al. New York: Springer Verlag, 1994.
5. Forrest, D.J. "Observations of Nuclear Emissions in Solar Flares." AIP Proceedings: New York, 211-216, (1988).
6. Murphy, R.J., et al., Astrophysical Journal (Suppl.) 63 (1987): 721-748.
7. Chupp, E. L., et al., Astrophysical Journal 318 (1987): 913-925.
8. Forman, M.A., et al, The Physics of the Sun, ed. P. A. Sturrock, T. E. Holzer, D.M. Mihalas, and R.K. Ulrich. 249-289. II. Dordrecht: D. Reidel, (1986).
9. Ramaty, R. and Mandzhavidze, N., 1994, in AIP Conf. Proc. 294, "High energy solar phenomena - a new era of spacecraft measurements", ed. J.M.Ryan and W.T. Vestrand (New York, AIP), p.26.
10. Debrunner, H., et al, 23rd International Cosmic Ray Conference in Calgary, Alberta, 115-118, 1993.
11. Ryan, J., et al., High-Energy Solar Phenomena—A New Era of Spacecraft Measurements in Waterville Valley, New Hampshire, AIP: New York, 89-93, (1994).
12. Share, G.H. , private comm., 1992.
13. Kanbach, G. , private comm., 1992.
14. Ryan, J.M., et al., Data Analysis in Astronomy edited by V. Di Gesú, Plenum Press: New York, 261-270, (1992).
15. Schönfelder, V., et al., Astrophysical Journal (Suppl. Series) 86 (1993): 657-692.
16. Frye, G.M., et al., 19th ICRC, **5**, 498, 1985
17. Frye, G.M., et al., 20th ICRC, **4**, 392, 1987
18. Pendleton et al., Workshop on Scint. Fiber Devel., Fermilab, 1093, 1988
19. Ansorge, R.E. et al., Nuclear instruments and Methods in Physics Research A265 (1988), 33-49
20. Hink, P.L., et al., Denver SPIE Proceedings, 1996
21. Morris, D., et al., J. Geophys. Res., 100 (A7), 12243 (1995)